Nano Research 2018, 11(1): 216–224
https://doi.org/10.1007/s12274-017-1621-4
Research Article
ISSN 1998-0124
CN 11-5974/O4

Facile growth of homogeneous $Ni(OH)_2$ coating on carbon nanosheets for high-performance asymmetric supercapacitor applications

Mingjiang Xie[1], Zhicheng Xu[1], Shuyi Duan[1], Zhengfang Tian[1,2], Yu Zhang[1], Kun Xiang[1], Ming Lin[3], Xuefeng Guo[1,2] (✉), and Weiping Ding[1] (✉)

[1] *Key Laboratory of Mesoscopic Chemistry of MOE, School of Chemistry & Chemical Engineering, Nanjing University, Nanjing 210023, China*
[2] *Hubei Key Laboratory for Processing and Application of Catalytic Materials, Huanggang Normal University, Huanggang 438000, China*
[3] *Institute of Materials Research and Engineering (IMRE), 2 Fusionopolis Way, Innovis, #08-03, Singapore 138634, Singapore*

Received: 23 January 2017
Revised: 8 April 2017
Accepted: 11 April 2017

KEYWORDS
in situ growth,
ion-exchange reaction,
hybrid $Ni(OH)_2$,
carbon nanosheet,
supercapacitor

ABSTRACT

The growth of a $Ni(OH)_2$ coating on conductive carbon substrates is an efficient way to address issues related to their poor conductivity in electrochemical capacitor applications. However, the direct growth of nickel hydroxide coatings on a carbon substrate is challenging, because the surfaces of these systems are not compatible and a preoxidation treatment of the conductive carbon substrate is usually required. Herein, we present a facile preoxidation-free approach to fabricate a uniform $Ni(OH)_2$ coating on carbon nanosheets (CNs) by an ion-exchange reaction to achieve the *in situ* transformation of a MgO/C composite to a $Ni(OH)_2$/C one. The obtained $Ni(OH)_2$/CNs hybrids possess nanosheet morphology, a large surface area (278 m^2/g), and homogeneous elemental distributions. When employed as supercapacitors in a three-electrode configuration, the $Ni(OH)_2$/CNs hybrid achieves a large capacitance of 2,218 F/g at a current density of 1.0 A/g. Moreover, asymmetric supercapacitors fabricated with the $Ni(OH)_2$/CNs hybrid exhibit superior supercapacitive performances, with a large capacity of 198 F/g, and high energy density of 56.7 Wh/kg at a power density of 4.0 kW/kg. They show excellent cycling stability with 93% capacity retention after 10,000 cycles, making the $Ni(OH)_2$/CNs hybrid a promising candidate for practical applications in supercapacitor devices.

1 Introduction

Because of their high power density, long cycling life, and high reliability, electrochemical capacitors (ECs, also named supercapacitors), have attracted considerable attention for energy storage applications [1, 2]. Generally,

Address correspondence to Xuefeng Guo, guoxf@nju.edu.cn; Weiping Ding, dingwp@nju.edu.cn

ECs can be classified as electric double layer capacitors (EDLCs) [3, 4] or pseudocapacitors based on their energy storage mechanism: EDLCs store charge through reversible adsorption/desorption of the electrolyte ions on/from the electrode surface, while pseudocapacitors deliver energy via fast reversible redox reactions at the surface. Whereas EDLCs with carbon-based electrodes can provide ultrahigh power density and excellent cycling life, their applications are limited by the poor energy density resulting from their low capacity. On the other hand, pseudocapacitors [5–8] based on electrochemically active transition metal hydroxides/oxides or polymers as electrode materials can potentially lead to much higher energy densities, as their redox reaction mechanism can provide a higher capacity compared to the EDLCs.

Among various pseudocapacitive materials, nickel hydroxide has long been intensively studied, owing to unique features such as high theoretical capacity, excellent redox behavior, ease of synthesis, large availability, low cost [9–13]. Despite these appealing features, the practical application of $Ni(OH)_2$ in ECs is still hindered by its poor cycling stability and low conductivity (~ 10^{-15} S/m). Regarding the poor cycling stability, recent investigations show that introducing non-electroactive components (e.g., Al, Zn, and Mg) in the nickel hydroxide matrix could result in a stable morphology/microstructure and thus an enhanced cycling life [14–16]. On the other hand, growth of $Ni(OH)_2$ on electrically conductive carbon-based substrates has proven to be an effective approach to address the issue of low conductivity [17–19]. As a result, nanocomposite structures consisting of pseudocapacitive materials grown on carbon are considered as the next-generation electrode materials for EC applications [20]. The fabrication of nanostructures consisting of a compact $Ni(OH)_2$ coating on a carbon substrate appears to be a suitable way to fully exploit the pseudocapacitance functionalities of $Ni(OH)_2$. However, the direct growth of a metal hydroxide/oxide coating on a carbon material is difficult, because their surfaces are not compatible [17]. Oxidative treatments of the carbon material are usually necessary to improve surface compatibility. However, these treatments can result in large numbers of structural defects and oxygen-containing groups, facilitating the growth of metal hydroxides/oxides on the carbon material surface, but at the same time reducing the conductivity of the substrate. Although many approaches including hydrothermal deposition [13, 18], solvothermal deposition [17], chemical precipitation [14], and hydrolysis [19] have been used to synthesize various $Ni(OH)_2$-carbon nanomaterials, not as many studies have concerned the direct growth of compact, homogeneous, and conformal $Ni(OH)_2$ coatings on carbon nanosheets (CNs) and the performance of these systems as asymmetric supercapacitors.

In this work, we introduce a simple and widely applicable strategy for the direct growth of a homogeneous $Ni(OH)_2$ coating on CNs. In this approach, illustrated in Fig. 1, a 30-nm-thick carbon nanosheet is initially grown on MgO via an incipient method, using a phenolic resin as the precursor and a sheet-like magnesium hydroxide (whose transmission electron microscopy (TEM) images are shown in Fig. S1 in the Electronic Supplementary Material (ESM)) as the template. Magnesium hydroxide is a widely adopted template for the synthesis of carbon-based electrode materials for energy storage and catalysis [21, 22] owing to its low cost and ease of removal. After carbonization, the obtained MgO/CNs composite was transferred to an aqueous solution containing Ni ions to undergo the following hydration and ion-exchange (IER) reactions

$$MgO(s) + H_2O \rightarrow Mg(OH)_2(s) \quad (1)$$

$$Mg(OH)_2(s) + Ni^{2+}(aq) \rightarrow Ni(OH)_2(s) + Mg^{2+}(aq) \quad (2)$$

After the IER, $Ni(OH)_2$ was grown *in situ* on the carbon nanosheets. This approach does not require oxidative treatment of the conductive carbon substrate to improve its surface compatibility, thus avoiding the loss of conductivity of the carbon substrate. The IER process also allows the simultaneous doping of the residual Mg component of magnesium hydroxide into the final $Ni(OH)_2$/CNs composite. The prepared $Ni(OH)_2$/CNs hybrid composite exhibits nanosheet morphology, large surface area (278 m^2/g), improved conductivity (~ 125 S/m), and homogeneous elemental distributions. Asymmetric supercapacitors prepared with the $Ni(OH)_2$/CNs hybrid exhibit superior supercapacitive performances, with a large capacity of

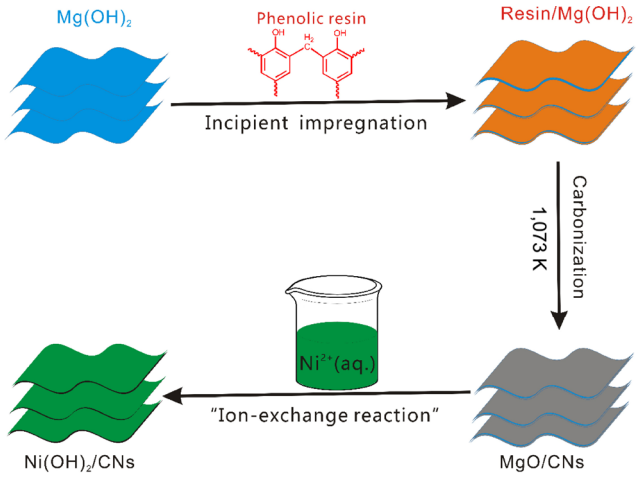

Figure 1 Schematic illustration of the growth of hybrid α-$Ni(OH)_2$ on carbon nanosheets.

198 F/g, high energy density of 68.6 Wh/kg, and excellent cycling stability (93% capacity retention) after 10,000 cycles.

2 Experimental

2.1 Synthesis of soluble phenolic resin

A precursor solution was prepared by dissolving 0.94 g phenol and 0.1 g NaOH in 10 mL distilled water. Then, 2.0 mL formaldehyde (37 wt.%) was added to the precursor solution followed by continuous stirring at 323 K for 6 h, which yielded a red-colored homogeneous solution of phenolic resin. Before using it as the starting material, the obtained phenolic resin was neutralized by diluted HCl.

2.2 Growth of $Ni(OH)_2$ on carbon nanosheets

A 10 mL amount of phenolic resin precursor solution was added to commercial $Mg(OH)_2$ with nanosheet morphology until an incipient state was reached. Subsequently, the obtained resin/template composite was heated at 373 K for 24 h to obtain a rigid composite by thermopolymerization. The rigid composite was heated to 1,073 K at a ramp rate of 2 K/min and carbonized in Ar for 4 h to obtain a carbon nanosheet/template composite. After carbonization, the obtained carbon nanosheet/MgO composite was immersed in 0.5 M $Ni(NO_3)_2$ solution for 48 h at room temperature to undergo the hydration and ion-exchange reactions. After the IER process, the obtained $Ni(OH)_2$/CNs composite was washed by filtration and dried at 373 K overnight. For comparison, CNs-free $Ni(OH)_2$ (denoted as $Ni(OH)_2$-IER) was fabricated by directly immersing MgO in 0.5 M $Ni(NO_3)_2$ solution for 48 h at room temperature, to undergo the hydration and ion-exchange reactions, following which the obtained $Ni(OH)_2$ was washed by filtration and dried at 373 K overnight.

2.3 Characterization

The morphology of the products was characterized by scanning electron microscopy (SEM, Hitachi S-4800). TEM and energy-dispersive X-ray spectroscopy (EDX) mapping images were obtained with a JEOL 2011 microscope operating at 200 kV. X-ray diffraction (XRD) patterns were recorded on a Philips X'Pert X-ray diffractometer with Cu Kα radiation (40 kV, 40 mA). N_2 adsorption–desorption isotherms were determined by a Micromeritics ASAP2020 analyzer. All samples were degassed at 573 K for 4 h before the measurements. The Raman spectra of the products were measured on a LabRAM Aramis spectrometer with a 532 nm laser as the excitation source. X-ray photoelectron spectra (XPS) were recorded on a Thermo ESCALAB 250 instrument using Al Kα radiation (15 kV, 150 W). All binding energies (BEs) were referenced to the C 1s peak at 284.6 eV. The composition of the products was determined by inductively coupled plasma atomic emission spectroscopy (ICP-AES, Optima 5300DV). Thermogravimetric and differential scanning calorimetry (TG-DSC) analyses were performed with a Netzsch STA 449 C instrument in air with a heating rate of 10 K/min. The four-probe method was employed to determine the powder conductivity of the samples, which were compressed into a dense disk under a pressure of 10 MPa.

2.4 Electrochemical tests

The electrochemical performances were measured in a three-electrode cell configuration in a 6.0 M KOH aqueous solution at room temperature, using Hg/HgO as the reference electrode and a platinum coil as the counter electrode. The working electrode was prepared by mixing the obtained $Ni(OH)_2$/CNs powder and polytetrafluoroethylene (PTFE) in a 90:10 mass ratio,

followed by transferring the resulting mixture onto a nickel foam and pressing it at 10 MPa.

In the case of the $Ni(OH)_2$-IER material, the working electrode was prepared by mixing the obtained $Ni(OH)_2$-IER powder, carbon black, and PTFE in a 70:25:5 mass ratio, followed by coating the resulting mixture onto nickel foam, before pressing it at 10 MPa. The electrochemical performances were determined by cyclic voltammetry (CV) and galvanostatic charge/discharge (GDC) curves. The specific capacitance (C_s, F/g) was calculated from the discharge curves according to

$$C_s = \frac{I\Delta t}{m\Delta V} \text{ (F/g)} \quad (3)$$

where I is the current density (A), Δt is the discharge time (s), m is the weight of active material (nickel hydroxide), and ΔV is the discharging potential window (V). The electrochemical properties of the asymmetric supercapacitor were investigated in a two-electrode cell configuration with the obtained $Ni(OH)_2$/CNs composite (mixed with 10% PTFE) as the positive electrode material, activated carbon (AC TF-B520, mixed with 10% carbon black and 10% PTFE) as the negative electrode material, and polypropylene film as separator, in 0.5 mL of 6.0 M KOH. The appropriate weight ratio of active materials ($Ni(OH_2$/CNs:TF-B520) needed to meet the charge balance of the two electrodes was estimated to be 1:3.2. The areal loadings of active materials for the positive and negative electrode were ~ 1.0 and ~ 3.2 mg/cm^2, respectively. Cyclic voltammetry and galvanostatic charge–discharge experiments were conducted on a CHI 660D electrochemical workstation (Shanghai CH Instrument Company, China). The specific capacitance of the asymmetric supercapacitor was calculated from the corresponding discharge curve according to Eq. (3), in which m was calculated as the total weight of the positive and negative electrodes. The energy densities and power densities were calculated according to $E = \frac{1}{2} \times \frac{1}{3.6} C_s V^2$ (Wh/kg) and $P = \frac{E}{t}$ (kW/kg), where V (V) is the working voltage of the cell and t is the discharge time.

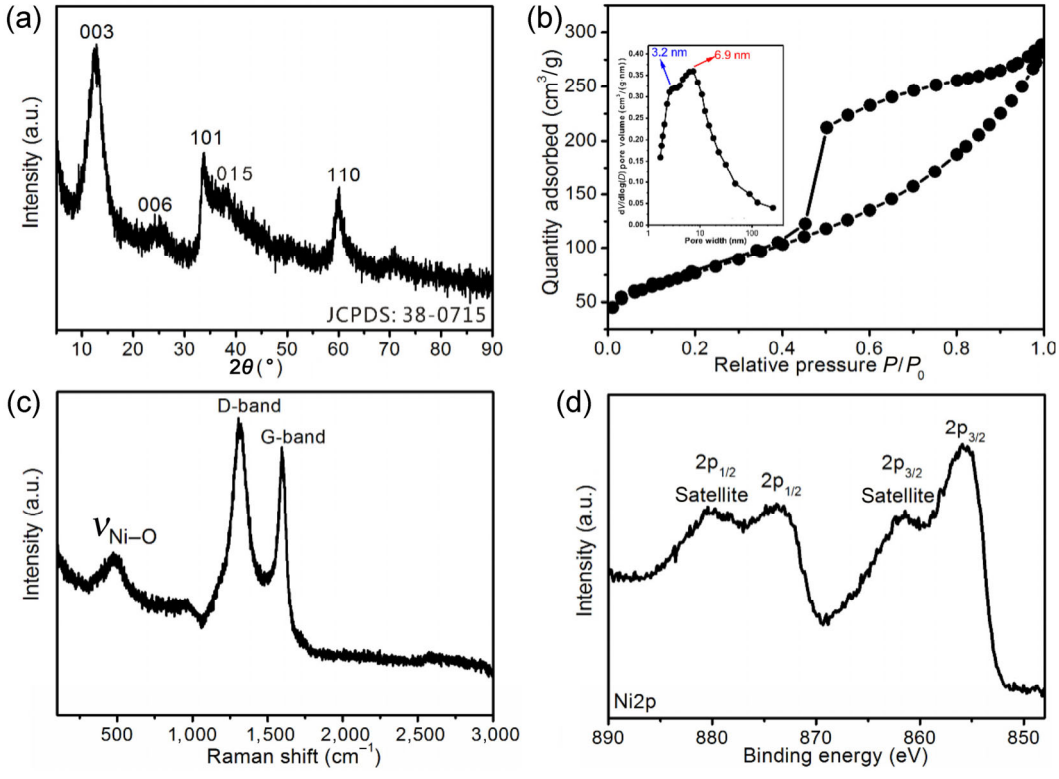

Figure 2 Structural analysis of the $Ni(OH)_2$/CNs hybrid. (a) XRD pattern; (b) N_2 sorption isotherms and pore size distributions (inset); (c) Raman spectra; (d) Ni 2p XPS spectra.

3 Results and discussion

The $Ni(OH)_2$/CNs hybrid was investigated by XRD, nitrogen sorption, Raman spectroscopy, and XPS. The XRD patterns (Fig. 2(a)) exhibits five diffraction peaks corresponding to the (003), (006), (101), (015), and (110) reflections of the single-crystalline phase of α-$Ni(OH)_2$ (JCPDS 38-0715). The nitrogen sorption isotherms (Fig. 2(b)) show type IV curves with a hysteresis loop, indicative of a mesoporous structure. The pore size distribution (PSD) curve shown in the inset of Fig. 2(b) shows that the obtained $Ni(OH)_2$/CNs composite has a wide pore size distribution centered at 6.9 nm with a shoulder at 3.2 nm.

The calculated Brunauer–Emmett–Teller (BET) surface area and pore volume listed in Table S1 in the ESM are 278 m^2/g and 0.56 cm^3/g, respectively. The Raman spectra (Fig. 2(c)) of the $Ni(OH)_2$/CNs composite shows three peaks at 450, 1,350, and 1,560 cm^{-1}. The peak around 450 cm^{-1} is ascribed to the Ni–O stretching vibration of $Ni(OH)_2$ [23], while the peaks at 1,350 and 1,560 cm^{-1} could be assigned to the D and G bands of graphitic carbon, respectively [24]. The Ni 2p XPS spectra (Fig. 2(d)) display four peaks at 855, 860, 873, and 878 eV that can be attributed to the Ni $2p_{3/2}$, Ni $2p_{3/2}$ (satellite), Ni $2p_{1/2}$, and Ni $2p_{1/2}$ (satellite) signals of $Ni(OH)_2$, respectively. The morphology of the fabricated $Ni(OH)_2$/CNs composite was characterized by SEM and TEM analysis. The SEM image in Fig. 3(a) shows that $Ni(OH)_2$/CNs is characterized by nanosheets with a thickness of ~ 35 nm and indicates that the thickness of the $Ni(OH)_2$ coating is ~ 2.5 nm (with a total thickness of ~ 5 nm including both top and bottom $Ni(OH)_2$ coatings). The nanosheet morphology was further confirmed by the TEM image in Fig. 3(b). The high-resolution TEM image in Fig. 3(c) and its corresponding fast Fourier transform (FFT)-filtered lattice image (Fig. 3(d)) display some visible lattice fringes with an identical interplanar distance of 0.232 nm, corresponding to the (015) planes of α-$Ni(OH)_2$, consistent with the XRD results.

To assess the homogeneity of the $Ni(OH)_2$ layer grown on the carbon substrate, elemental mapping analysis was conducted by scanning transmission electron microscopy (STEM). Figure 4 shows the STEM image and the corresponding elemental mapping of

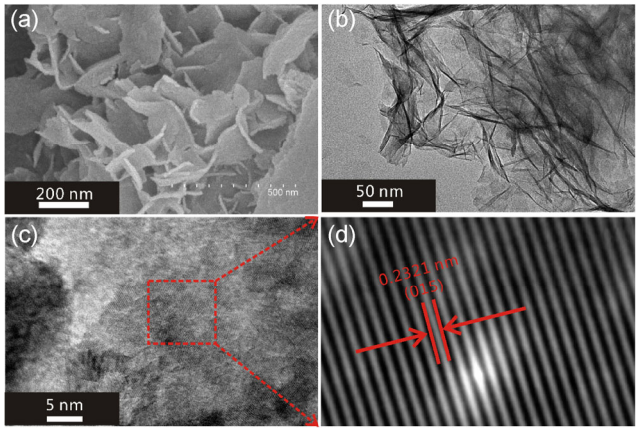

Figure 3 Morphology characterization. (a) SEM, (b) TEM, and (c) HRTEM images of $Ni(OH)_2$/CNs; (d) FFT-filtered lattice image corresponding to the rectangular area highlighted in (c).

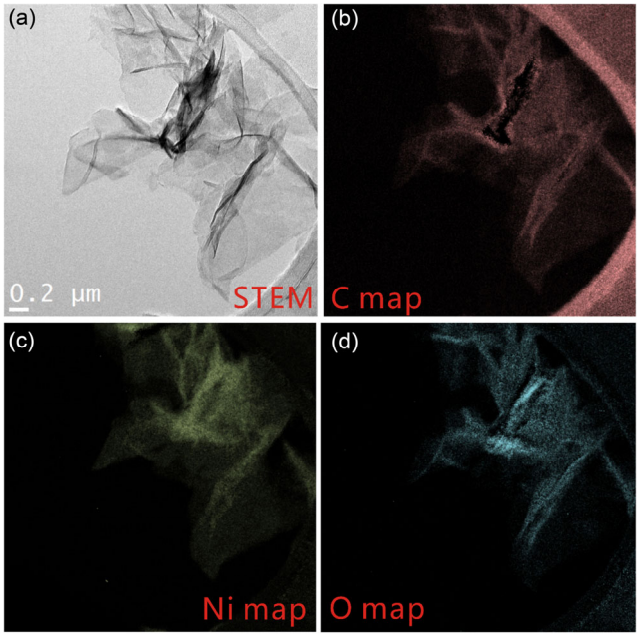

Figure 4 Morphology and elemental distribution analysis of $Ni(OH)_2$/CNs. (a) STEM image and corresponding elemental maps of C (b), Ni (c), and O (d).

the $Ni(OH)_2$/CNs hybrid. The C, Ni, and O maps are analogous to those of the original STEM image, indicative of a homogeneous $Ni(OH)_2$ coating on the CNs, further confirming the successful homogeneous growth of $Ni(OH)_2$ on the nanosheets. To investigate the percentage of $Ni(OH)_2$ in the $Ni(OH)_2$/CNs composite, TG-DSC analysis was carried out under air. As shown in Fig. S2 in the ESM, the DSC curve of $Ni(OH)_2$/CNs shows two endothermic peaks around

350 and 580 K, ascribed to the desorption of adsorbed water and to the phase transformation from nickel hydroxide to nickel oxide, respectively. Another visible exothermic peak around 630 K can be attributed to the combustion of the carbon substrate. Consistent with the DSC curve, three weight loss stages emerge in the TG curve with a total weight loss of 68%, from which the weight percentage of $Ni(OH)_2$ in the composite can be estimated as 73%.

The elemental composition of hybrid $Ni(OH)_2$ was determined by ICP-AES, in which the molar ratio of Ni/Mg is 13:1.

The electrochemical capacitive performance of the obtained $Ni(OH)_2$/CNs composite was initially studied in a three-electrode configuration in 6.0 M KOH. Figure S3(a) in the ESM shows the cyclic voltammograms of the composite at various scan rates, which reveal a typical pseudocapacitive behavior with redox peaks around 0.5 and 0.3 V, ascribed to the Faradaic reaction $Ni(OH)_2 + OH^- \rightarrow NiOOH + H_2O + e^-$.

The GDC curves of $Ni(OH)_2$/CNs at current densities ranging from 1.0 to 20 A/g (Fig. S3(b) in the ESM) show an obvious deviation from the typical triangular shape associated with non-Faradaic EDLCs, further demonstrating the Faradaic characteristics of charge storage in the present systems. Figure S3(c) in the ESM shows the specific capacitance of $Ni(OH)_2$/CNs and $Ni(OH)_2$-IER calculated from the GDC curves. The capacitances of $Ni(OH)_2$/CNs, calculated for current densities between 1.0 and 20 A/g, are 2,218 (1 A/g), 2,106 (2 A/g), 2,032 (5 A/g), 1,936 (10 A/g), and 1,605 F/g (20 A/g), respectively. At each current density, the measured capacitance of $Ni(OH)_2$/CNs exceeds that of $Ni(OH)_2$-IER (whose maximum capacitance is 1,855 F/g). The corresponding electrochemical impedance spectroscopy (EIS) measurements of the two $Ni(OH)_2$ electrodes were analyzed through the Nyquist plots shown in Fig. S4 in the ESM. These plots show that the two $Ni(OH)_2$ electrodes have almost the same high-frequency slope, indicative of a similar ion diffusion process. However, at low frequency, the $Ni(OH)_2$/ CNs hybrid shows a smaller semicircle loop diameter than the CNs-free $Ni(OH)_2$-IER, implying a faster charge transfer in $Ni(OH)_2$/CNs, consistent with the much higher conductivity of $Ni(OH)_2$/CNs. The EIS analysis reveals that the superior capacitance of $Ni(OH)_2$/CNs compared with $Ni(OH)_2$-IER can be attributed to its unique structure, in which the compact $Ni(OH)_2$ coating on the CNs results in a larger electroactive surface area and thus provides a higher capacitance.

To assemble an asymmetric supercapacitor, commercial AC TF-B520 with a surface area of 1,999 m^2/g (Fig. S5 in the ESM) was adopted as negative electrode. Figure S3(d) in the ESM shows the cyclic voltammograms of TF-B520 under various scan rates; all plots exhibit a rectangular-shaped curve indicative of EDLC behavior, with a maximum capacitance of 230 F/g. To enlarge the voltage window [25], an asymmetric supercapacitive cell (ASC) was assembled using the prepared $Ni(OH)_2$/CNs as positive electrode and the AC TF-B520 as the negative electrode, as detailed in the Experimental section.

The performance of the ASC was evaluated by the cyclic voltammograms and GDC curves measured within a potential window of 0–1.6 V. All voltammograms of the $Ni(OH)_2$/CNs composite (Fig. 5(a)) at scan rates from 10 to 200 mV/s show an anodic peak at 1.1 V and a cathodic peak at 0.8 V assigned to the redox reaction $Ni(OH)_2 + OH^- \rightarrow NiOOH + H_2O + e^-$.

The GDC curves in Fig. 5(b) also indicate the occurrence of redox reactions, in agreement with the CV measurements. Figure 5(c) shows the capacity of the entire device, including both positive and negative electrodes, calculated from the GDC curves via Eq. (3), where m was calculated as the total weight of the positive and negative electrodes. The calculated capacities were 196 (1 A/g), 173 (2 A/g), 152 (5 A/g), 135 (10 A/g), 123 F/g (20 A/g), respectively. As shown in Table S2 in the ESM, the capacity of the ASC fabricated with the $Ni(OH)_2$/CNs hybrid (192 F/g) is higher than that of some recently reported $Ni(OH)_2$ nanostructures, e.g., $Ni(OH)_2$/reduced graphene oxide (RGO) (182 F/g) [18], pure $Ni(OH)_2$ (98 F/g) synthesized by a hydrothermal method with hexamethylenetetramine as precipitation reagent [16], Mg-$Ni(OH)_2$ grown on nickel foam (167 F/g) [16]. The higher capacity of the $Ni(OH)_2$/CNs composites can be attributed to the unique two-dimensional structure coated on the carbon substrate, which provides wide pathways for electrolyte diffusion and continuous channels for fast electron transport (leading to a much higher

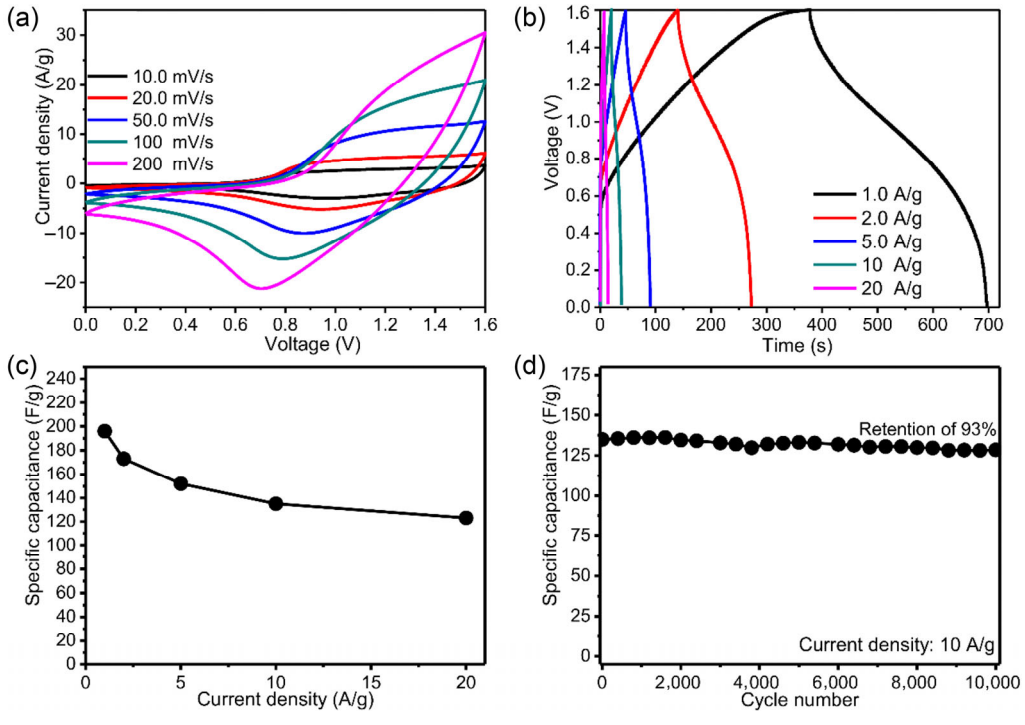

Figure 5 Electrochemical performance of an asymmetric supercapacitor based on the hybrid $Ni(OH)_2$/CNs electrode. (a) Cyclic voltammograms recorded at various scan rates, (b) charge/discharge curves at different current densities, (c) specific capacitances at different current densities, and (d) cycling test performed for 10,000 cycles at a current density of 10 A/g.

conductivity) and thus allows fully exploiting the pseudocapacitance functionalities of $Ni(OH)_2$. To evaluate the cycling stability of the assembled ASC, a continuous charge/discharge test was conducted at a current density of 10 A/g. As shown in Fig. 5(d), after 10,000 cycles the capacitance of the ASC remains as high as 132 F/g with a retention of ~ 93%, indicative of an excellent cycling stability. The superior cycling stability of the ASC based on the $Ni(OH)_2$/CNs composite can be attributed to the stable morphology/microstructure resulting from the synergistic effect of the doped magnesium hydroxide and the carbon substrate. The good ASC performances of devices based on $Ni(OH)_2$/CNs electrodes are also reflected by their energy and power densities, as shown in the Ragone plot (Fig. 6). The maximum energy density (E_{max}) of the $Ni(OH)_2$/CNs was estimated as 68.6 Wh/kg at 1.58 kW/kg, which is is much higher than that of $Ni(OH)_2$/graphene (53.3 Wh/kg at 1.72 kW/kg) [19], pure $Ni(OH)_2$ (33.9 Wh/kg at 1.58 kW/kg) [16], and Mg-$Ni(OH)_2$ (57.9 Wh/kg at 1.58 kW/kg) [16], and it is also one of the highest values recorded among recently reported asymmetric supercapacitors based on nanostructured $Ni(OH)_2$ (whose E_{max} values are listed in Table S2 in the ESM). The superior supercapacitor performances and excellent cycling life of the present systems can be ascribed to the open nanostructure, Mg ion hybridization, and large surface area of $Ni(OH)_2$ grown on the CNs, which ensures a stable microstructure/morphology and provides a higher number of electrochemically active surface sites for redox reactions.

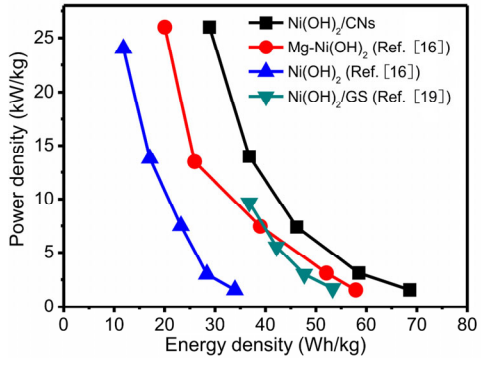

Figure 6 Ragone plot of energy and power densities of the obtained $Ni(OH)_2$/CNs, compared with previously reported results for devices fabricated using various nickel hydroxide compounds as the working electrode.

4 Conclusions

A versatile approach was developed to fabricate a hybrid nickel hydroxide composite by *in situ* direct growth of $Ni(OH)_2$ on carbon nanosheets, using ion-exchange reactions with magnesium hydroxide as the sacrificial material and dopant. The obtained hybrid $Ni(OH)_2$/CNs composites possess nanosheet morphology, large surface area (278 m^2/g), and homogeneous elemental distributions. An asymmetric supercapacitor based on the hybrid $Ni(OH)_2$/CNs exhibit superior supercapacitive performances, with a large capacity of 198 F/g, high energy density of 68.6 Wh/kg, and excellent cycling stability (93% retention) after 10,000 cycles, making the present composites promising candidates for practical applications in supercapacitor devices. Moreover, the simple strategy developed in this work is widely applicable to the growth of other nanostructured metal hydroxides/oxides on a carbon substrate, with potential applications in fields such as energy storage and catalysis, among others.

Acknowledgements

This work was financially supported by the National Natural Science Foundation of China (Nos. 20773063, 20773062, 21173119, and 21273109), the Fundamental Research Funds for the Central Universities. The authors also thank the support from the Hubei Key Laboratory for Processing and Application of Catalytic Materials (No. CH201401).

Electronic Supplementary Material: Supplementary material (TEM image of $Mg(OH)_2$; TG-DSC curves $Ni(OH)_2$/CNs; structural parameters of $Ni(OH)_2$CNs, pure $Ni(OH)_2$ and AC; electrochemical capacitive performances of $Ni(OH)_2$/CNs and AC tested in three-cell configuration; nitrogen sorption isotherms and PSD curve of AC; comparison table of the asymmetric supercapacitor performances of the $Ni(OH)_2$/CNs in our work and the recent nickel hydroxides nanostructures from literatures) is available in the online version of this article at https://doi.org/10.1007/s12274-017-1621-4.

References

[1] Wu, H.; Jiang, K.; Gu, S. S.; Yang, H.; Lou, Z.; Chen, D.; Shen, G. Z. Two-dimensional $Ni(OH)_2$ nanoplates for flexible on-chip microsupercapacitors. *Nano Res.* **2015**, *8*, 3544–3552.

[2] Hu, Y. T.; Guan, C.; Ke, Q. Q.; Yow, Z. F.; Cheng, C. W.; Wang, J. Hybrid Fe_2O_3 nanoparticle clusters/rGO paper as an effective negative electrode for flexible supercapacitors. *Chem. Mater.* **2016**, *28*, 7296–7303.

[3] Chi, Y.-W.; Hu, C.-C.; Shen, H.-H.; Huang, K.-P. New approach for high-voltage electrical double-layer capacitors using vertical graphene nanowalls with and without nitrogen doping. *Nano Lett.* **2016**, *16*, 5719–5727.

[4] Zhao, J.; Lai, H. W.; Lyu, Z. Y.; Jiang, Y. F.; Xie, K.; Wang, X. Z.; Wu, Q.; Yang, L. J.; Jin, Z.; Ma, Y. W. et al. Hydrophilic hierarchical nitrogen-doped carbon nanocages for ultrahigh supercapacitive performance. *Adv. Mater.* **2015**, *27*, 3541–3545.

[5] Xu, Y. X.; Huang, X. Q.; Lin, Z. Y.; Zhong, X.; Huang, Y.; Duan, X. F. One-step strategy to graphene/$Ni(OH)_2$ composite hydrogels as advanced three-dimensional supercapacitor electrode materials. *Nano Res.* **2013**, *6*, 65–76.

[6] Liang, D. W.; Wu, S. L.; Liu, J.; Tian, Z. F.; Liang, C. H. Co-doped Ni hydroxide and oxide nanosheet networks: Laser-assisted synthesis, effective doping, and ultrahigh pseudocapacitor performance. *J. Mater. Chem. A* **2016**, *4*, 10609–10617.

[7] Liu, X. Y.; Gao, Y. Q.; Yang, G. W. A flexible, transparent and super-long-life supercapacitor based on ultrafine Co_3O_4 nanocrystal electrodes. *Nanoscale* **2016**, *8*, 4227–4235.

[8] Zhu, J. W.; Chen, S.; Zhou, H.; Wang, X. Fabrication of a low defect density graphene-nickel hydroxide nanosheet hybrid with enhanced electrochemical performance. *Nano Res.* **2012**, *5*, 11–19.

[9] Le Comte, A.; Brousse, T.; Belanger, D. New generation of hybrid carbon/$Ni(OH)_2$ electrochemical capacitor using functionalized carbon electrode. *J. Power Sources* **2016**, *326*, 702–710.

[10] Zhang, C. Q.; Chen, Q. D.; Zhan, H. B. Supercapacitors based on reduced graphene oxide nanofibers supported $Ni(OH)_2$ nanoplates with enhanced electrochemical performance. *ACS Appl. Mater. Interfaces* **2016**, *8*, 22977–22987.

[11] Shi, D.; Zhang, L.; Yin, X.; Huang, T. J.; Gong, H. A one step processed advanced interwoven architecture of $Ni(OH)_2$ and Cu nanosheets with ultrahigh supercapacitor performance. *J. Mater. Chem. A* **2016**, *4*, 12144–12151.

[12] Wang, R. H.; Jayakumar, A.; Xu, C. H.; Lee, J.-M. $Ni(OH)_2$ nanoflowers/graphene hydrogels: A new assembly for supercapacitors. *ACS Sustainable Chem. Eng.* **2016**, *4*, 3736–3742.

[13] Min, S. D.; Zhao, C. J.; Zhang, Z. M.; Chen, G. R.; Qian, X. Z.; Guo, Z. P. Synthesis of $Ni(OH)_2$/RGO pseudocomposite on nickel foam for supercapacitors with superior performance. *J. Mater. Chem. A* **2015**, *3*, 3641–3650.

[14] Chen, X.; Long, C. L.; Lin, C. P.; Wei, T.; Yan, J.; Jiang, L. L.; Fan, Z. J. Al and Co co-doped α-$Ni(OH)_2$/graphene hybrid materials with high electrochemical performances for supercapacitors. *Electrochim. Acta* **2014**, *137*, 352–358.

[15] Lee, G.; Varanasi, C. V.; Liu, J. Effects of morphology and chemical doping on electrochemical properties of metal hydroxides in pseudocapacitors. *Nanoscale* **2015**, *7*, 3181–3188.

[16] Xie, M. J.; Duan, S. Y.; Shen, Y.; Fang, K.; Wang, Y. Z.; Lin, M.; Guo, X. F. *In-situ*-grown $Mg(OH)_2$-derived hybrid α-$Ni(OH)_2$ for highly stable supercapacitor. *ACS Energy Lett.* **2016**, *1*, 814–819.

[17] Ma, X. W.; Li, Y.; Wen, Z. W.; Gao, F. X.; Liang, C. Y.; Che, R. C. Ultrathin β-$Ni(OH)_2$ nanoplates vertically grown on nickel-coated carbon nanotubes as high-performance pseudocapacitor electrode materials. *ACS Appl. Mater. Interfaces* **2015**, *7*, 974–979.

[18] Liu, Y. H.; Wang, R. T.; Yan, X. B. Synergistic effect between ultra-small nickel hydroxide nanoparticles and reduced graphene oxide sheets for the application in high-performance asymmetric supercapacitor. *Sci. Rep*. **2015**, *5*, 11095.

[19] Wang, H. L.; Casalongue, H. S.; Liang, Y. Y.; Dai, H. J. $Ni(OH)_2$ nanoplates grown on graphene as advanced electrochemical pseudocapacitor materials. *J. Am. Chem. Soc*. **2010**, *132*, 7472–7477.

[20] Patil, U.; Lee, S. C.; Kulkarni, S.; Sohn, J. S.; Nam, M. S.; Han, S.; Jun, S. C. Nanostructured pseudocapacitive materials decorated 3D graphene foam electrodes for next generation supercapacitors. *Nanoscale* **2015**, *7*, 6999–7021.

[21] Tang, C.; Wang, H.-S.; Wang, H.-F.; Zhang, Q.; Tian, G.-L.; Nie, J.-Q.; Wei, F. Spatially confined hybridization of nanometer-sized NiFe hydroxides into nitrogen-doped graphene frameworks leading to superior oxygen evolution reactivity. *Adv. Mater*. **2015**, *27*, 4516–4522.

[22] Li, M. M.; Tang, M. H.; Deng, J.; Wang, Y. Nitrogen-doped flower-like porous carbon materials directed by *in situ* hydrolysed MgO: Promising support for Ru nanoparticles in catalytic hydrogenations. *Nano Res.* **2016**, *9*, 3129–3140.

[23] Li, W.; Xin, L. P.; Xu, X.; Liu, Q. D.; Zhang, M.; Ding, S. J.; Zhao, M. S.; Lou, X. J. Facile synthesis of three-dimensional structured carbon fiber-$NiCo_2O_4$-$Ni(OH)_2$ high-performance electrode for pseudocapacitors. *Sci. Rep.* **2015**, *5*, 9277.

[24] Xie, M. J.; Yang, J.; Liang, J. Y.; Guo, X. F.; Ding, W. P. *In situ* hydrothermal deposition as an efficient catalyst supporting method towards low-temperature graphitization of amorphous carbon. *Carbon* **2014**, *77*, 215–225.

[25] Yan, J.; Fan, Z. J.; Sun, W.; Ning, G. Q.; Wei, T.; Zhang, Q.; Zhang, R. F.; Zhi, L. J.; Wei, F. Advanced asymmetric supercapacitors based on $Ni(OH)_2$/graphene and porous graphene electrodes with high energy density. *Adv. Funct. Mater*. **2012**, *22*, 2632–2641.